

Multi-scale temporal variation of methane flux and its controls in a subtropical tidal salt marsh in eastern China

Hong Li · Shengqi Dai · Zutao Ouyang · Xiao Xie · Haiqiang Guo ·
Caihong Gu · Xiangming Xiao · Zhenming Ge · Changhui Peng ·
Bin Zhao

Received: 30 May 2017 / Accepted: 6 December 2017
© Springer International Publishing AG, part of Springer Nature 2018

Abstract CH₄ emissions could vary with biotic and abiotic factors at different time scales. However, little is known about temporal dynamics of CH₄ flux and its controls in coastal marshes. In this study, CH₄ flux was continuously measured with the eddy covariance technique for 2 years in a subtropical salt marsh in eastern China. Wavelet analysis was applied to explore the multi-scale variations of CH₄ flux and its controls. Additionally, partial wavelet coherence was used to disentangle confounding effects of measured

variables. No consistent diurnal pattern was found in CH₄ fluxes. However, the hot-moments of CH₄ flux were observed after nighttime high tide on days near the spring tide. Periodic dynamics were also observed at multi-day, semilunar and seasonal scales. Tide height in summer had a negative effect on CH₄ flux at the semilunar scale. Air temperature explained most variations in CH₄ fluxes at the multi-day scale but CH₄ flux was mainly controlled by PAR and GEP at the seasonal scale. Air temperature explained 48% and 56% of annual variations in CH₄ fluxes in 2011 and 2012, respectively. In total, the salt marsh acted as a CH₄ source ($17.6 \pm 3.0 \text{ g C-CH}_4 \text{ m}^{-2} \text{ year}^{-1}$), which was higher than most studies report for inland wetlands. Our results show that CH₄ fluxes exhibit multiple periodicities and its controls vary with time

Responsible Editor: Maren Voss.

Electronic supplementary material The online version of this article (<https://doi.org/10.1007/s10533-017-0413-y>) contains supplementary material, which is available to authorized users.

H. Li · S. Dai · X. Xie · H. Guo · X. Xiao · B. Zhao (✉)
Ministry of Education Key Laboratory for Biodiversity
Science and Ecological Engineering, and Coastal
Ecosystems Research Station of the Yangtze River
Estuary, Fudan University, Shanghai 200438, China
e-mail: zhaobin@fudan.edu.cn

H. Li · C. Peng
Department of Biology Science, Institute of Environment
Sciences, University of Quebec at Montreal,
Montreal C3H 3P8, Canada

Z. Ouyang
Department of Geography, Michigan State University,
East Lansing, MI, USA

C. Gu
Hydrological Station of Chongming County, Shanghai,
China

X. Xiao
Department of Botany and Microbiology, Center for
Spatial Analysis, University of Oklahoma, Norman, OK,
USA

Z. Ge
State Key Laboratory of Estuarine and Coastal Research,
East China Normal University, Shanghai 200062, China

scale; moreover, CH₄ flux is strongly modified by tide. This study emphasizes the importance of ecosystem-specific measurements of CH₄ fluxes, and more work is needed to estimate regional CH₄ budgets.

Keywords CH₄ flux · Tide height · Wavelet analysis · Eddy covariance

Introduction

Wetlands are the dominant natural source of atmospheric methane (CH₄) and have profound effects on atmospheric CH₄ concentration dynamics in recent decades (Bridgman et al. 2013; Kirschke et al. 2013). Many studies have estimated global wetland CH₄ fluxes (F_{CH₄}), but with great uncertainties (IPCC 2013), mainly due to the lack of detailed information on temporal dynamics of F_{CH₄} and its mechanistic drivers. Ecosystem-specific continuous measurements of F_{CH₄} are important to capture the high spatial and temporal variability in wetlands (Nicolini et al. 2013). While salt marshes have high rates of carbon sequestration (Chmura et al. 2003), they can act as sources of CH₄ (Chanton and Whiting 1996; Holm et al. 2016; Poffenbarger et al. 2011). Thus, there is an urgent need to obtain ecosystem-specific information on methane emission dynamics and to refine the understanding of its controls in tidal salt marshes.

Several studies have attempted to investigate temporal F_{CH₄} dynamics and its controls in wetlands over the last decade (see Table S1 for some examples, which was modified from Koebsch et al. (2015)), with most studies focusing on dynamics on diurnal and seasonal scales. Some studies have found diurnal cycles of F_{CH₄}, which could be related to temperature, plant-mediated transport, and root exudation (references in Table S1). Seasonal variations were mostly controlled by temperature and water table level (references in Table S1). To date, few studies have analyzed ecosystem F_{CH₄} and its corresponding regulating factors on multiple temporal scales (Hatala et al. 2012; Koebsch et al. 2015; Sturtevant et al. 2015), with a lack of studies on tidal salt marshes. In addition, potential confounding effects on F_{CH₄} among those environmental drivers, such as temperature and photosynthetic active radiation (PAR), were rarely

disentangled (Hatala et al. 2012; Sturtevant et al. 2015).

Compared to inland wetlands, a specific hydrological process—tidal activity with different periods compared to temperature and radiation—can affect CH₄ emissions in coastal wetlands. Tidal cycling has the potential to affect F_{CH₄} via various ways, such as sulfate, water level, and physical action of the ebbing and flowing of tides in salt marshes. The flood tide often brings sulfate into coastal wetlands, leading to an increase in salinity and sulfate content from the neap tide to spring tide in some marshes (Bu 2013; Tong et al. 2013). The presence of SO₄²⁻ in salt marshes as a more favorable terminal electron acceptor can competitively suppress CH₄ production based on thermodynamics (Holm et al. 2016; Neubauer et al. 2013; Poffenbarger et al. 2011; Weston et al. 2014). Water level changes have complex and interacting effects on many processes influencing F_{CH₄} (Christensen et al. 2003; Christensen et al. 1997; Homineltenberg et al. 2014; Long et al. 2010). Generally, a high water-table level promotes anaerobic conditions conducive to the production of CH₄ and limits the zone of aerobic oxidation of CH₄ within the soil. However, a rapid drop of water table can release CH₄ from pore water and result in a large episodic burst of F_{CH₄} (Bubier and Moore 1994; Windsor et al. 1992). Moreover, there are only few studies observing a direct relationship between tide cycle and F_{CH₄} by using chamber technique. On the one hand, Tong et al. (2013) found that CH₄ emissions on neap tide days were higher than those on spring tide days, which was also observed by Bu et al. (2015). On the other hand, Yamamoto et al. (2009) reported that diurnal variations of F_{CH₄} were positively correlated to water table depth during spring tide. On the contrary, Tong et al. (2013) concluded that F_{CH₄} was significantly related to soil temperature and not to tide height, salinity, or redox potential at the diel scale. These studies improved our understanding of F_{CH₄} in coastal wetlands, but due to the deficiencies of the chamber technique, which does not provide continuous ecosystem-scale F_{CH₄} (e.g. during tidal inundations), the processes regulating F_{CH₄} in tidal salt marshes remain unclear.

The eddy covariance (EC) technique represents a direct and quasi-continuous measurement technique integrating turbulent fluxes over the scale of ecosystems with minimal disturbance (Baldocchi et al.

2001). The widespread application of EC has greatly improved our understanding of the biogeochemical processes driving greenhouse gas fluxes (Baldocchi 2014; Chu et al. 2014; Hatala et al. 2012). However, there were very few studies that measured F_{CH_4} in tidal salt marshes using the EC technique (Holm et al. 2016). Wavelet coherence allows us to obtain the correlation between two signals both in the time and frequency domain and yields the phase shift between the signals, which is a meaningful criterion for a potential cause-and-effect relationship (Grinsted et al. 2004; Hatala et al. 2012; Koebsch et al. 2015; Stoy et al. 2005; Vargas et al. 2010). Particularly, this time series analysis tool can separate the tidal effect on F_{CH_4} as its semi-diurnal and semi-lunar periods differ from other environmental variables in tidal salt marshes. Moreover, the comparison of wavelet coherence and partial wavelet coherence can help disentangle confounding effects (Ng and Chan 2012; Ouyang et al. 2014), and multiple wavelet coherence is capable of determining the resulting coherence of multiple independent variables on a dependent variable. Although wavelet analysis shows great potential for promoting our mechanistic understanding of ecosystem processes, these time series analysis approaches have yet been rarely applied to investigate time scale-specific controls on F_{CH_4} (but see few exceptions in Hatala et al. (2012), Xu et al. (2014), Koebsch et al. (2015) and Sturtevant et al. (2015)), and have never been used for F_{CH_4} in salt marshes.

For the first time, we investigate F_{CH_4} from a subtropical tidal salt marsh in China derived with the EC technique using wavelet analyses. The main objectives of this study are: (1) to determine annual budgets of F_{CH_4} from the salt marsh; (2) to analyze the variation in characteristics and time scale-specific regulating factors of F_{CH_4} . As tide acts as an important hydrological process in tidal salt marshes, we particularly investigate the role of tidal activity in regulating F_{CH_4} .

Materials and methods

Study site

Our study site (31°31′0.12″N, 121°57′38.52″E) is a part of the FLUXNET network (CMW3 in Fig. 1), located in the Dongtan wetland of Chongming Island,

northeast of Shanghai city, China (Fig. 1). Given the large amounts of sediment (mostly silt with grain size of 4–13 μm) delivered by the Yangtze River, the wetland continues to expand at a rate of 64 m per year toward the East China Sea (Zhao et al. 2008). The climate is a subtropical monsoon climate, and mean temperature and annual precipitation were 17.1 °C and 868–1532 mm from 1991 to 2012, respectively. The dominant plant species are *Phragmites australis* and *Spartina alterniflora*. The study area is affected by semidiurnal and semilunar tidal activity, with tidewater salinity ranging between 0 ppt (part per thousand) and 25 ppt between 2005 and 2007. While, soil sulfate content was between 0.2 and 1.2 ppt with an average of 0.7 ppt in 2010 (Bu 2013).

Flux and ancillary data

The eddy covariance (EC) technique was used to quantify carbon dioxide flux (F_{CO_2}) and F_{CH_4} between the tidal salt marsh and atmosphere from March 23, 2011 to December 3, 2012. Sensors were mounted 5 m above the soil surface. Sensor height was determined to ensure that the EC system is mounted at least twice the height of the plant canopy (1.5–2.5 m) during the peak growing season. The EC system included a sonic anemometer [CSAT3, Campbell Sci., Inc., Logan, UT, USA (CSI)], an open path $\text{CO}_2/\text{H}_2\text{O}$ infrared gas analyzer [LI7500A, LI-COR, Cor., Lincoln, NE, USA (LI-COR)], and an open path CH_4 gas analyzer (LI7700, LI-COR) during March 23 to April 16, 2012. The CSAT3 was then replaced by a Gill Windmaster Pro sonic anemometer (Gill Instruments Limited, Lymington, Hampshire, United Kingdom). The raw data were sampled with a frequency of 10 Hz and recorded by a CR5000 data logger. Additionally, nighttime (approximately 0:00 am–8:00 am) data were missing for lack of electrical power supply between September 13 and December 3 in 2012.

F_{CO_2} and F_{CH_4} were calculated using EddyPro (Version 5.1.1, www.licor.com/eddypro). The advanced settings included angle of attack corrections for Gill WindMaster Pro, despiking, time lag detection, double coordinate rotation, spectral correction, compensation of density fluctuations (WPL terms), instrument sensible heat adjustment for LI7500A, steady state test, and the well-developed turbulence test (for detailed information see Text S1 and Fig. S1).

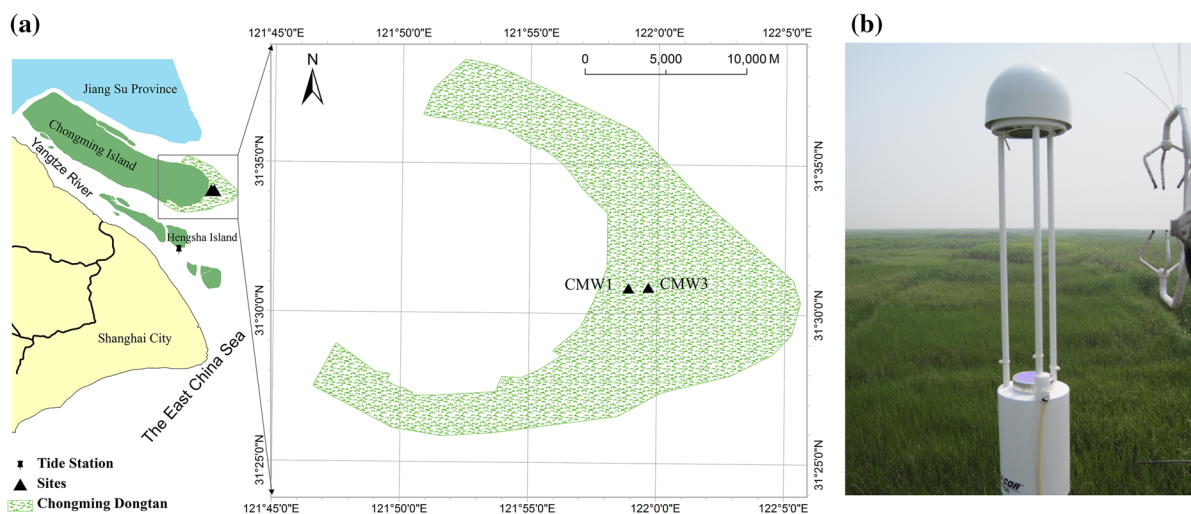


Fig. 1 Location (a) and a photo (b) of the study site (CMW3, Chongming Wetland 3). The shaded areas (a) labeled Chongming Dongtan is a salt marsh. (Color figure online)

The relative signal strength indicator (RSSI) was adopted to filter for periods when the mirror of LI7700 was contaminated by rainfall or dust ($\text{RSSI} < 20\%$). Data were removed when rainfall occurred. In addition, to ensure well-developed mixing conditions, we used friction velocity (u^*) as a criterion for atmospheric mixing (Reichstein et al. 2005), and applied a threshold of $u^* > 0.15 \text{ m s}^{-1}$. The steady state test and the well-developed turbulence test were used as quality flags (Foken et al. 2004). The test (Foken et al. 2004) (1–9 system) provided the flag “1 ~ 3” for high quality fluxes, “4 ~ 6” for intermediate quality fluxes, and “9” for poor quality fluxes. Thus, only data for which the quality flag was < 7 were used for further analysis. These quality criteria and occasionally occurring sensor failures led to gaps of different duration. For the entire observation period, the remaining data coverage was 46% for F_{CO_2} and 44% for F_{CH_4} .

Micrometeorological variables were also measured (details are listed in Table S2), including long-/short-wave radiation, PAR, air temperature, relative humidity, and precipitation. Tidal data were measured at the nearest tide station (Hengsha station, $31^\circ 17' 36'' \text{N}$, $121^\circ 50' 54'' \text{E}$, approximately 25 km distant of our flux tower). The mean and maximum tide ranges above the Wusong Datum Plane (zero reference level for sea level with widespread use in the Yangtze River basin) were 2.0–3.1 and 4.6–6.0 m during the study period, respectively (Yang et al. 2001). We measured the tide

height at the EC tower station for almost half year and found that there was a certain time lag between the tower location and Hengsha tidal station, which rarely exceeded one half hour (Xie et al. 2013). The semi-diurnal tide, including an entire flooding and ebbing process, is characterized by a period of about 12 h. Therefore, there are commonly two high tides and two low tides each day. Heights of high and low tides change from day to day, with a period of about 15 days. This periodic variation is defined as a semi-lunar tidal cycle, including neap and spring tide periods. The intertidal zone can be inundated by tidewater for several days during the spring tide period. Meanwhile, on the neap tide day, tidal heights are relatively low, thus most of the vegetated zone is unaffected by tidewater.

Gap filling and partitioning

Gaps in F_{CO_2} were filled using the marginal distribution sampling method, and were further partitioned into gross ecosystem production (GEP) and ecosystem respiration (ER) following Reichstein et al. (2005). The above partitioning was implemented online (<http://www.bgc-jena.mpg.de/~MDIwork/eddyproc/>), and variables such as DOY (day of year), time of day, R_g (global radiation), T_a (air temperature), RH (relative humidity), VPD (vapor pressure deficit), u^* (friction velocity), and P (precipitation) were used. Both GEP and ER are presented with positive signs

($F_{CO_2} = ER - GEP$). The meteorological variables (Ta, RH, precipitation) were gap-filled using regressions with complimentary data from adjacent sites (CMW1, 1000 m distant) or using linear interpolation for short gaps within 24 h.

F_{CH_4} was gap-filled using the artificial neural network (ANN) approach, which is an expanded version of the Matlab “nnstart”. For training the network, we used the following variables as potential drivers of CH_4 : four fuzzy sets of seasons, Ta, PAR, RH, rainfall, air pressure, u^* , u (u wind speed), TH (tide height) and maximum of TH. Season was coded using four fuzzy variables (winter, spring, summer and fall) each having a value between 0 and 1 depending on the time of year (Järvi et al. 2012; Papale and Valentini 2003). A two-layer feed-forward network with sigmoid hidden neurons and linear output neurons was used to obtain a fitting model. Ten eligible models were chosen for prediction. The mean of the ten model predictions was used for the calculation of the annual balance (for more details, see Text S2). And the standard deviation was used to estimate the uncertainty in the gap-filling.

Wavelet analyses

Continuous wavelet transform (CWT) was used to investigate periodicities of F_{CH_4} . We deployed wavelet coherence (WTC) to quantify the relationship between F_{CH_4} and one variable. Moreover, partial wavelet coherence (PWC) was used to identify the coherence between F_{CH_4} and one variable after eliminating the confounding effect of other variables. At last, we used multiple wavelet coherence (MWC) to assess the resulting coherence of multiple independent variables on F_{CH_4} .

We used the CWT with Morlet wavelet (Grinsted et al. 2004) to investigate the spectral characteristics of F_{CH_4} and the variables of interest. The WTC spectrum is interpreted as the local correlation between two variables in frequency-time space (Grinsted et al. 2004). $R(x, y)^2$ is defined as the WTC of two time series x and y (Grinsted et al. 2004). The WTC allows us to examine whether or not the highest coherency areas in the frequency domain have a consistent phase angle, which indicates a phase-locked relationship between two variables. For time periods with significant wavelet coherence, we used the phase angle to calculate the time lag (timelag = phase

angle* $wavelength/2\pi$) between the correlated oscillations of the two series. The relative phase relationship is shown as arrows (with in-phase pointing right, anti-phase pointing left. Arrows pointing up are interpreted as X leading Y by 270° or lagging Y by 90°).

The PWC is a technique similar to partial correlation that facilitates the identification of the resulting WTC between two time series y and x_1 after eliminating the influence of their common dependent time series x_2 (Ng and Chan 2012). The PWC squared (after the removal of the effect of x_2) can be defined by an equation similar to the partial correlation squared, as follows:

$$RP^2(y, x_1, x_2) = \frac{|R(y, x_1) - R(y, x_2) \times R(y, x_1)|^2}{[1 - R(y, x_2)]^2 [1 - R(x_2, x_1)]}, \quad (1)$$

which ranges from 0 to 1, like the simple WTC. R is the WTC operator in (1). In this case, a low PWC squared shown at the position of a high wavelet coherence squared implies that the time series x_1 does not have a significant influence on the time series y at that particular time–frequency space, and time series x_2 dominates the effect on the variance of y , and vice versa for the opposite case. If both $RP^2(y, x_1, x_2)$ and $RP^2(y, x_2, x_1)$ continue to have significant bands, both x_1 and x_2 have significant influences on y .

The MWC is an extension of the bivariate case to the multivariate case. In this case, the correlation of the variables with each other is taken into account when calculating coherency. The MWC operates in a similar manner to multiple correlation, in that it is capable of assessing the resulting coherence of multiple independent variables on a dependent variable. The application of MWC can be defined with the following equation:

$$RM^2(y, x_2, x_1) = \frac{R^2(y, x_1) + R^2(y, x_2) - 2\text{Re}[R(y, x_1) \times R(y, x_2) \times R(x_2, x_1)]}{1 - R^2(x_2, x_1)}, \quad (2)$$

which provides the resulting wavelet coherence squared that computes the proportion of wavelet power of the dependent time series y that is explained by the two independent variables x_1 and x_2 at a given time and frequency. R is the WTC operator in (2). Since MWC is very sensitive to the dependencies of a time series, the assurance of the independence of x_1

and x_2 is necessary before conducting MWC (Ng and Chan 2012). In the present study, the WTC of tide height & Ta and tide height & PAR showed only few significant regions indicating that they were mostly independent. Considering that Ta and PAR/GEP are not independent from each other, they cannot be used together for MWC analyses.

We applied CWT, WTC based on the software package provided by Grinsted et al. (2004). The PWC, and MWC analyses were based on the software package provided by Ng and Chan (2012). A 5% significance level against red noise was tested through Monte Carlo simulations for CWT, WTC, PWC and MWC (Grinsted et al. 2004; Mihanović et al. 2009; Ng and Chan 2012). Gaps in F_{CH_4} were filled with the mean of the normalized data instead of using the ANN approach, similar to Hatala et al. (2012) and Ouyang et al. (2014), thereby avoiding spurious correlations between F_{CH_4} and the variables of interest. To simplify, we defined the range of the five general time scales in this study as follows (Figs. 4, 5, 6): (1) hourly scale (2^{1-2} half hours, 1–2 h), representing perturbations such as passing clouds and turbulent scales up to intervals of 30 min; (2) diel scale (2^{3-6} half hours, 4 h to 1.3 days), representing the day-night cycle of sunlight, PAR, temperature, and tide; (3) multi-day scale (2^{7-9} half hours, 2.6–10.7 days), identifying synoptic weather variability and variations in temperature; (4) half-to-one-month scale (2^{9-11} , 10.7–42.7 days), representing tide cycle between spring tide and neap tide; (5) seasonal scale (2^{11-13} , 42.7–170.7 days), representing the annual solar cycle and phenology (referring to Sturtevant et al. (2015)).

Results

Environmental conditions during the study period

Both air temperature and PAR showed distinct seasonal variations. Annual (July 1, 2011–June 30, 2012) mean air temperature and total rainfall were 16.2 °C and 886.9 mm, respectively. According to field observations, most of the flux footprint area was flooded when the tide height was > 3.7 m. There were 364 (58.4%) of 623 days with a maximum height of the high tide reaching 3.7 m. Variations in tide height showed quasi-semidiurnal and quasi-semilunar cycles. Although the seasonal or annual amplitude of

variations were relatively small, the seasonal-averaged tide height in summer was higher than in other seasons (Fig. S2).

Diurnal variation, seasonal variation, and annual budget of F_{CH_4}

The study site was a source of CH_4 during the measurement period (Fig. 2a). The annual (July 1, 2011–June 30, 2012) median and mean of half-hourly F_{CH_4} were 40.8 and 58.6 $\text{nmol m}^{-2} \text{s}^{-1}$, respectively. Daily mean F_{CH_4} values were positive throughout the study period (Fig. 2a, green lines), except for six days. Few negative half-hourly F_{CH_4} were observed during the measurement period (Fig. 2a), such as in August 2012 at around noon. After gap-filling, the annual (July 1, 2011–June 30, 2012, according to the amount of high quality data) carbon loss as CH_4 was $17.6 \pm 3.0 \text{ g C-CH}_4 \text{ m}^{-2} \text{ year}^{-1}$ and annual carbon uptake as CO_2 was estimated to be $637.6 \pm 52.4 \text{ g C-CO}_2 \text{ m}^{-2} \text{ year}^{-1}$, resulting in a net carbon uptake of $-620 \text{ g C m}^{-2} \text{ year}^{-1}$ by the marsh.

F_{CH_4} exhibited a distinct seasonal pattern, with larger emissions during the growing season than during the non-growing season (Fig. 2a). At the start of the growing season in April, F_{CH_4} increased continuously and peaked at $0.27 \text{ g m}^{-2} \text{ day}^{-1}$ on 7th July 2011 and $0.47 \text{ g m}^{-2} \text{ day}^{-1}$ on 10th July 2012.

From hourly to monthly scales, the pattern of F_{CH_4} differed from that of F_{CO_2} . No consistent pattern of diurnal variations in F_{CH_4} was observed at the tidal salt marsh (Fig. 3a), unlike for F_{CO_2} , which exhibited significantly strong oscillations at a diel scale during the growing season (Fig. 3b). Spectral peaks of F_{CH_4} were also observed at the multi-day scale (e.g., 5.3 days), half-to-one-month scale (e.g., 10.7 days to 21.3 days), and seasonal scale (between 42.7 and 170.7 days) (Fig. 3a).

Regulation of F_{CH_4}

Correlations between F_{CH_4} and several potential driving variables (see Table S1) were tested using traditional correlation analysis and WTC analyses. Since no significance or little significant regions in the time–frequency domain between VPD, u^* , LE, and air pressure and F_{CH_4} were observed, these variables were not used for further analyses in this study.

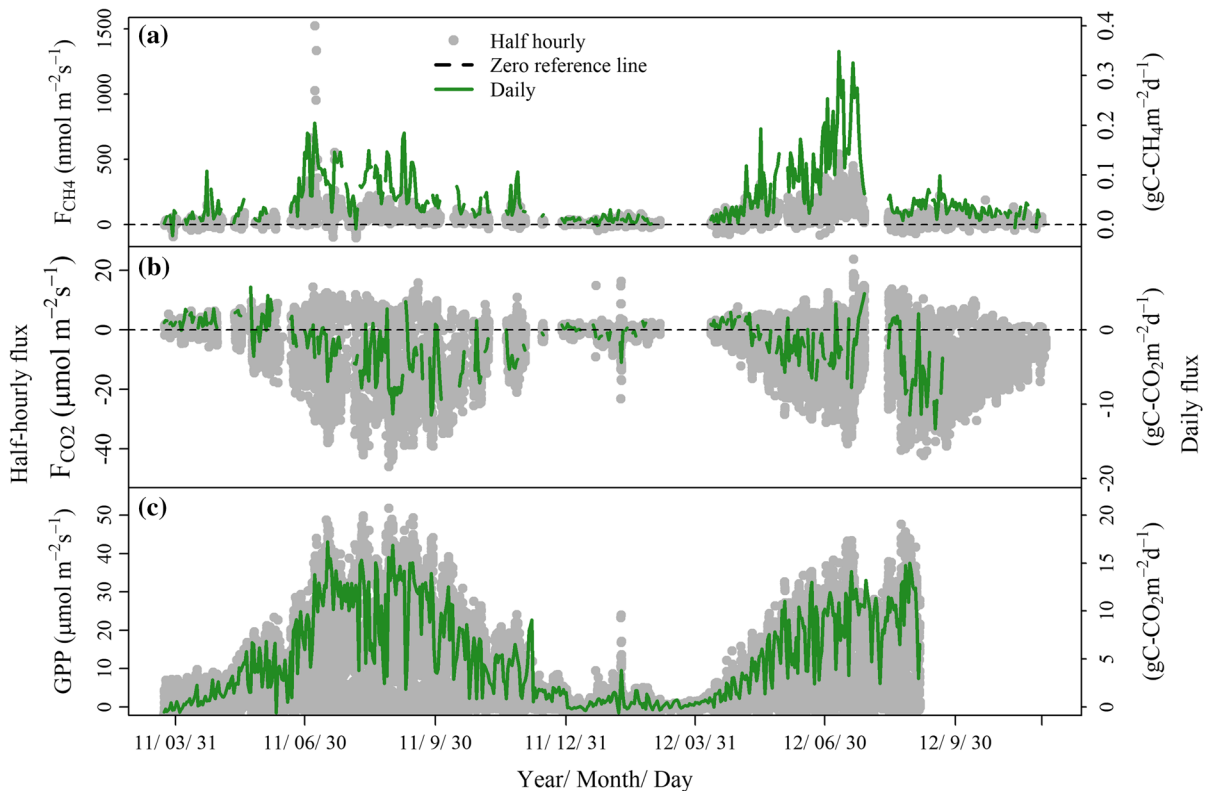


Fig. 2 Time series of half-hourly (gray circles) and daily (green lines) fluxes, including (a) net ecosystem CH_4 exchange (F_{CH_4}), (b) net ecosystem CO_2 exchange (F_{CO_2}), (c) gross ecosystem photosynthesis (GEP). Half-hourly zero reference lines (black dotted lines) for right Y axis were added (a, b). Between 13

September and 3 December in 2012, daily F_{CO_2} was not calculated (b), and thus, GEP (c) were not estimated as nighttime (approximately 0:00 am–8:00 am) data were missing for lack of electrical supply. (Color figure online)

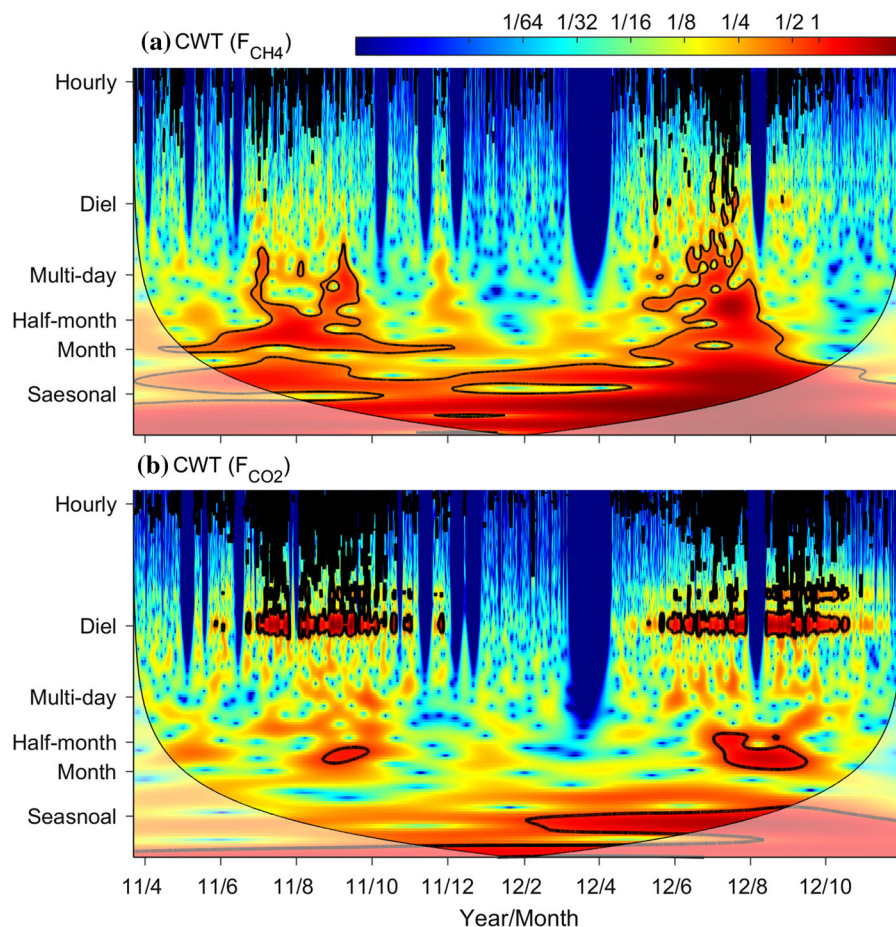
Wavelet coherence analysis showed that Ta, PAR, GEP and TH were significantly correlated to F_{CH_4} , whereas these environmental and biological variables played different roles at each scale (Fig. 4). At the diel scale, all four environmental variables significantly co-varied with F_{CH_4} at some time domains, but these significant areas were discontinuous (Fig. 4). At longer time scales, the significant phase-locked area of F_{CH_4} with Ta was located at a multi-day scale with in-phase relationship (Fig. 4a); F_{CH_4} and TH was located at the half-to-one-month scale with a constant or slowly changing anti-phase relationship, particularly between June and September, 2011 (Fig. 4c). Tide height led F_{CH_4} by ca. 0.7 days at the half-to-one-month scale. Additionally, the significant phase-locked areas of F_{CH_4} and PAR (Fig. 4b), GEP (Fig. 4d) were located at both the multi-day scale and the seasonal scale. Large data gaps in March and August in 2012 may be the primary reason for less

significant phase-locked areas in WTC of F_{CH_4} with GEP or TH during 2012.

The effect of Ta on F_{CH_4} confounded the effect of PAR on F_{CH_4} at the multi-day scale. After eliminating the effect of Ta on PAR and F_{CH_4} by the analysis of PWC (F_{CH_4} , Ta, PAR), almost all the significant regions in WTC (PAR, F_{CH_4}) (Fig. 4b) disappeared (F_{CH_4} , PAR, Ta) at the multi-day scale (Fig. 5b). In contrast, after eliminating the effect of PAR on Ta and F_{CH_4} , the significant regions in WTC (Ta, F_{CH_4}) (Fig. 4a) remained in PWC (F_{CH_4} , Ta, PAR) at the multi-day scale (Fig. 5a). Moreover, the PWC (F_{CH_4} , Ta, PAR) squared was comparable to the WTC (Ta, F_{CH_4}) at the multi-day scale. The results of PWC (F_{CH_4} , Ta, GEP) were similar to PWC (F_{CH_4} , Ta, PAR). Thus, Ta rather than PAR or GEP dominates the effect on the variance of F_{CH_4} at the multi-day scale.

The combination of TH, Ta and PAR explained most variations of F_{CH_4} from diel to seasonal scales.

Fig. 3 Continuous wavelet transform for methane flux (F_{CH_4}) (a) and carbon dioxide flux (F_{CO_2}) (b) time series. The 5% significance level against red noise is shown as a black thick contour. The cone of influence (COI) is shown as a thin line. The blue vertical stripes are the result of long data gaps. The degree of red color indicates the wavelet power. (Color figure online)



At the diel scale, as a result of the combined impact on F_{CH_4} , the significant areas of MWC (F_{CH_4} , TH, Ta) (Fig. 6a) and MWC (F_{CH_4} , TH, PAR) (Fig. 8b) were much larger than that of any single variable in Fig. 4. From the diel-to-month scales, the areal extent and amplitude of significant regions of MWC (F_{CH_4} , TH, PAR) (Fig. 6b) were not comparable to those of MWC (F_{CH_4} , TH, Ta) (Fig. 6a). Thus, TH and Ta collectively provide a better explanation for the variability of F_{CH_4} than using TH and PAR from diel-to-month scales. In contrast, TH and PAR collectively explained more variability of F_{CH_4} from month to seasonal scales (Fig. 6). In summary, TH collectively with Ta and PAR explained most of the variability of F_{CH_4} from diel to seasonal scales, even though Ta and PAR played different roles at each scale (Fig. 6).

Exponential regression analysis was adopted to reveal the annual controls on F_{CH_4} . Annually, F_{CH_4} exhibited exponential dependence on air temperature

(Fig. 7, $R^2 = 0.48$ and 0.56 in 2011 and 2012, respectively).

Tidal effects on F_{CH_4}

To better illustrate the tidal effect on the variability of F_{CH_4} at half-to-one-month scales, non-gap-filled high quality (quality flags < 4) data for 31 days (July to August, DOY 191–222), including two full cycles of spring and neap tides, are analyzed (Fig. 8). The highest daily tide heights were above 3.7 m during most days, indicating that the flux footprint was flooded during these days (Fig. 8). Daily-averaged F_{CH_4} gradually increased from spring to neap tide and decreased from neap to spring tide, except for the days after a heavy rainfall event. After the heavy rainfall on DOY 215 (2 days after the spring tide), F_{CH_4} decreased over the next two days (Fig. 8). Nevertheless, F_{CH_4} started increasing before the day of neap

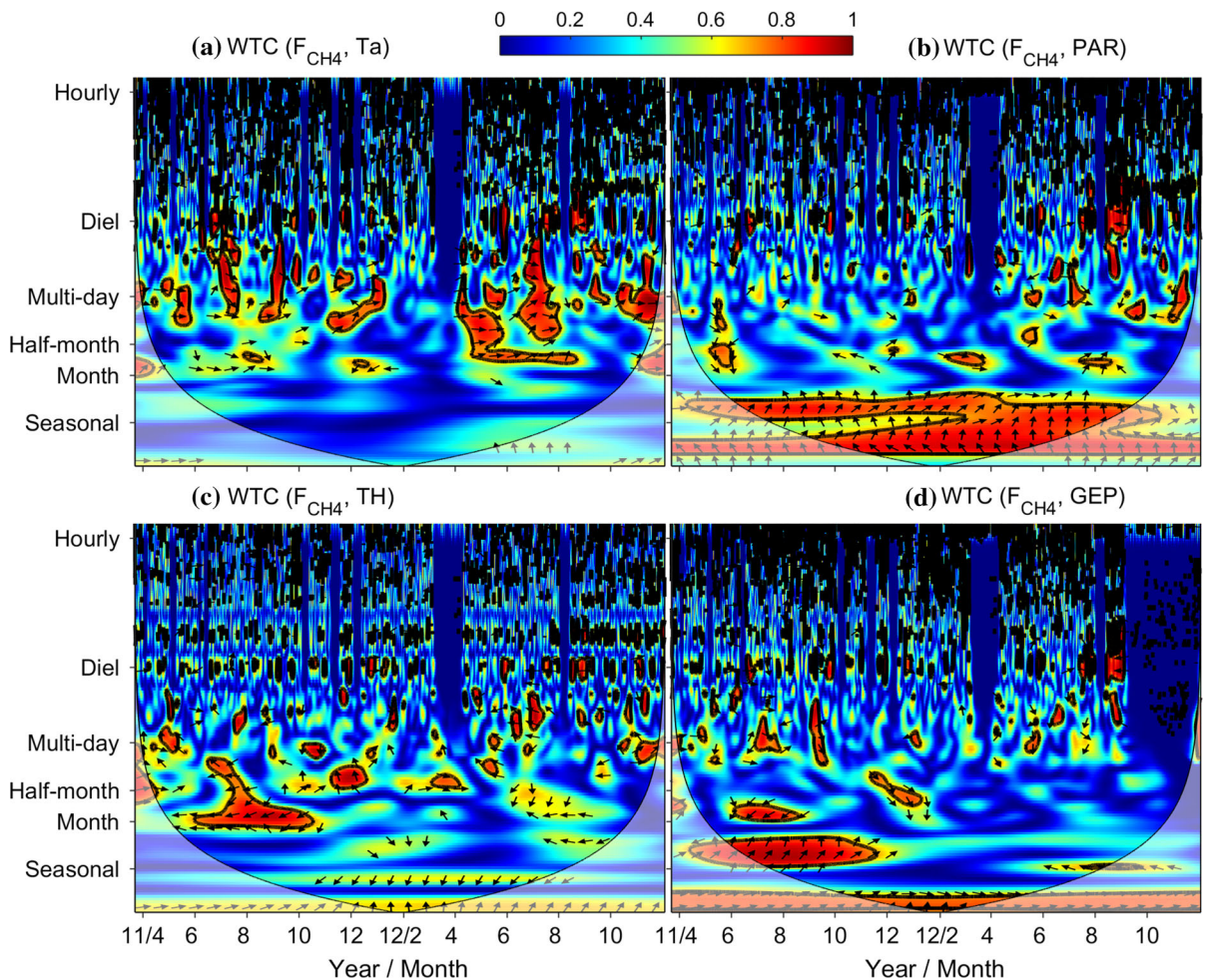


Fig. 4 Wavelet coherence (WTC) of methane flux (F_{CH_4}) with air temperature (Ta) (a), PAR (b), tide height (c), GEP (d). The 5% significance level against red noise is shown as a thick contour. The cone of influence (COI) is shown as a thin line. The relative phase relationship is shown as arrows. The degree of red color indicates the strength of the localized determination coefficient (wavelet coherence R^2 closely resembles that

of a traditional coefficient of determination) in time frequency space. 1 (red) means the two signals are highly correlated and 0 (blue) means no correlation. The relative phase relationship is shown as arrows (with in-phase pointing right, anti-phase pointing left. Arrows pointing up are interpreted as X [e.g. Ta (a), PAR (b), tide height (c), GEP (d)] leading Y (e.g. F_{CH_4}) by 270° or lagging Y by 90°). (Color figure online)

tide arrived as expected (Fig. 8). In other words, F_{CH_4} was significantly negatively correlated to the daily maximum tide height ($p < 0.001$, $R^2 = 0.58$), but not to Ta ($p > 0.05$) or GEP ($p > 0.05$).

Hot moments of CH_4 emissions occurred after the high tide height. Considering that there was a disturbance of heavy rainfall during the period of DOY191–222, the data of another tidal cycle (DOY 182 to 190) were added for diel F_{CH_4} dynamic analysis. But these data were not used for statistical analysis (e.g. daily average), due to data gaps (Fig. 9). For periods near the spring tide, large CH_4 emission pulses were

observed after the high tide (convert to ebb tide) on 2–3 days (DOY 182–183, 197–198 and 211) before the spring tide and 1–4 days (DOY 186–189, 201–204 and 214–217) after the spring tide (Fig. 9). We defined these large emissions, with greater than threefold standard deviation + average of F_{CH_4} within ± 6 h, as hot moments in this study. There were 17 days (81%) of the 21 days near the spring tide days with CH_4 hot moments, while no pulse emissions were observed on the neap tide days. Moreover, all of these CH_4 hot moments on these days occurred 2–5 h after the nighttime high tide. The timing of these hot-

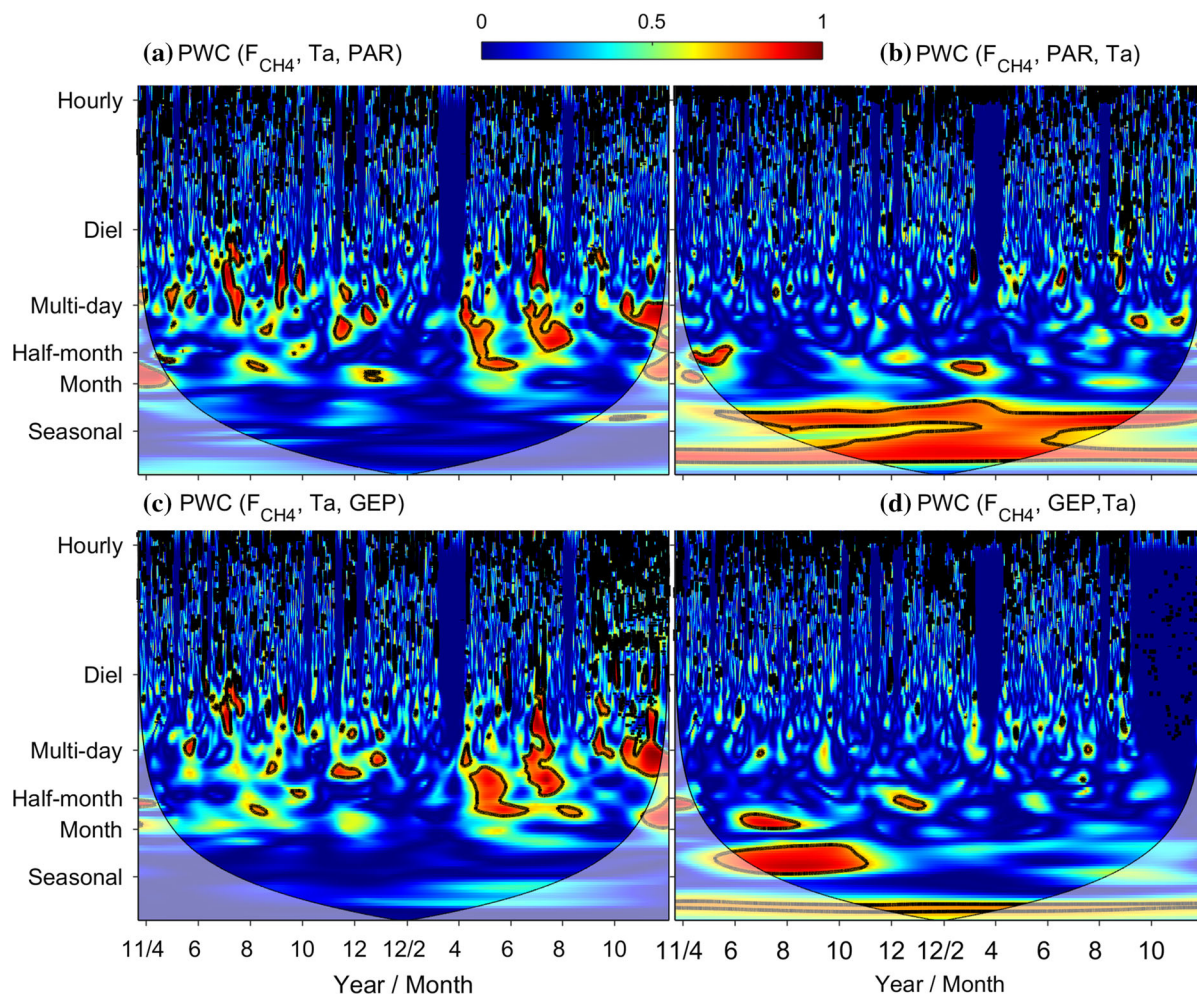


Fig. 5 Partial wavelet coherence (PWC) (F_{CH_4} , Ta, PAR) (a), PWC (F_{CH_4} , PAR, Ta) (b), PWC (F_{CH_4} , Ta, GEP) (c) and PWC (F_{CH_4} , GEP, Ta) (d). The result in (a, c) showed the coherence between F_{CH_4} and Ta after removing the effect of the time series PAR (a) or GEP (c). Similarly, the effect of the time series Ta was eliminated in the results of the coherence between F_{CH_4} and

PAR (b), F_{CH_4} and GEP (d). The 5% significance level against red noise is shown as a thick contour. The cone of influence (COI) is shown as a thin line. The sections marked by red color indicate high correlation between the two variables. (Color figure online)

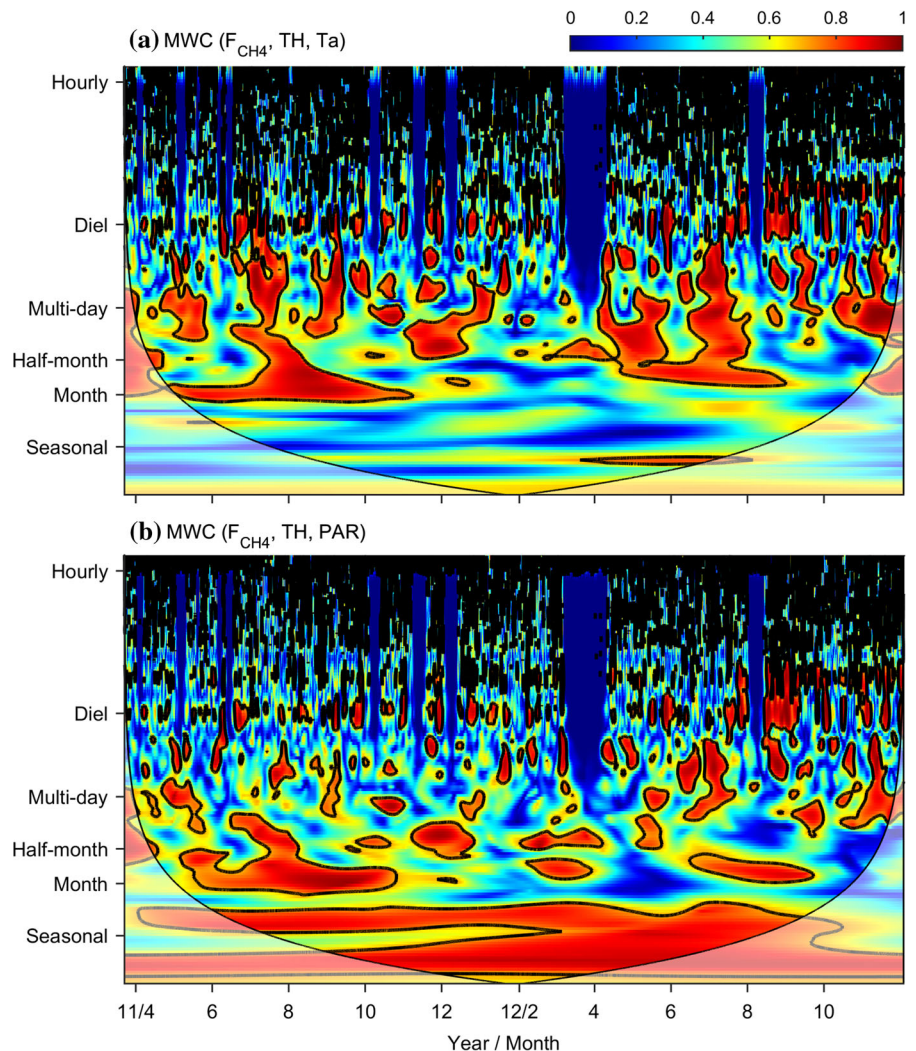
moments changed with the timing of the high tide. For example, when the high tide appeared at 23:30 and 24:00 of DOY 182 and 183, respectively, the hot moments of DOY 182 and 183 occurred at 2:00 and 1:30, respectively (Fig. 9). One day before and on the spring tide day (DOY 184–185, 199–200, 212–213), F_{CH_4} was gradually decreased to the lowest value until the ebb of tide (DOY 186, 201 and 214) (Fig. 9). The episodic fluxes were up to 11-fold of the daily mean, and thus removal of these episodic fluxes would reduce the daily estimation up to 30% (e.g. DOY 187, 188).

Discussion

Magnitude of F_{CH_4} over the tidal salt marsh

The annual mean half-hourly F_{CH_4} at the tidal salt marsh was higher (mean and median: 38.1 and 57.9 $\text{nmol m}^{-2} \text{s}^{-1}$) than most of the F_{CH_4} reported for inland wetlands (see Table S3). Nicolini et al. (2013) concluded that 50% of reported average fluxes obtained by the micrometeorological approach fell between 11.02 and 68.48 $\text{nmol m}^{-2} \text{s}^{-1}$, with a median of 24.24 $\text{nmol m}^{-2} \text{s}^{-1}$. However, most of

Fig. 6 Multiple wavelet coherence (MWC) of methane flux (F_{CH_4}) ~ tide height + air temperature (Ta) (a), MWC of F_{CH_4} ~ tide height + PAR (b). The 5% significance level against red noise is shown as a thick contour. The cone of influence (COI) is shown as a thin line. The sections marked by red color indicate high correlation between F_{CH_4} and these multiple variables. (Color figure online)



those measurements were conducted in boreal regions (Nicolini et al. 2013).

As reviewed by Poffenbarger et al. (2011), mesohaline (salinity: 5 ~ 18 ppt) marshes had average methane emissions of $12.3 \pm 8.25 \text{ g C-CH}_4 \text{ m}^{-2} \text{ year}^{-1}$, which was close to but slightly lower than our current study ($17.6 \text{ g C-CH}_4 \text{ m}^{-2} \text{ year}^{-1}$). Another annual estimate of F_{CH_4} with the EC technique [$10.35 \text{ g C-CH}_4 \text{ m}^{-2} \text{ year}^{-1}$; (Holm et al. 2016)] was also lower than our study. Reported annual F_{CH_4} show a wide range as wetlands differ in their biological and environmental conditions. A study of the northern Yellow River estuary with a higher salinity exhibited a smaller magnitude of methane emission (Sun et al. 2013a). Moreover, CH_4 emissions from the marshes dominated by vascular plants appear

to be higher than those of marshes dominated by other vegetation types (Table S4) (Sun et al. 2013a, b).

Remarkably, the hot moments of F_{CH_4} were captured by the EC technique in a tidal salt marsh for the first time. Although there was no consistent diurnal pattern of F_{CH_4} during the measurement period, we found hot moments of methane flux after nighttime high tide on the days near the spring tide. This phenomenon has not been reported by studies in the same region (Bu 2013; Bu et al. 2015) or in a similar marsh near the study site (Cheng et al. 2010; Cheng et al. 2007). On the contrary, in another subtropical tidal salt marsh, Tong et al. (2010) found that CH_4 emissions during the flooding and ebbing process were significantly lower than before flooding and after ebbing, and no large hot moments of methane

Fig. 7 Daily average methane fluxes against air temperature throughout the year together with the line indicating the temperature dependence. The data are grouped into 2011 (gray points) and 2012 (black circles), and separate model parameters are fitted for 2011 (green lines) and 2012 (red lines). (Color figure online)

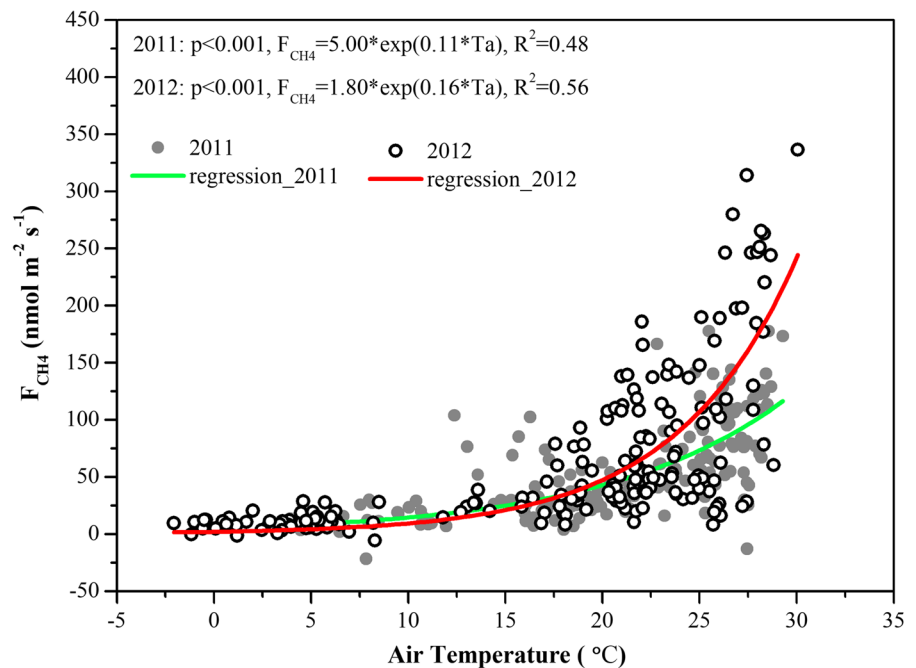
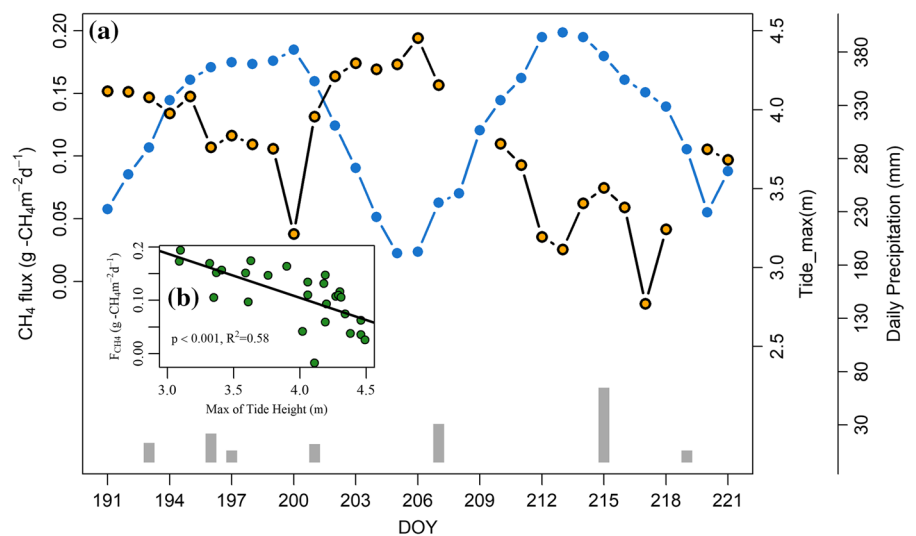


Fig. 8 Daily methane flux (F_{CH_4}) without gap-filling (a, black dotted line with orange bgcolor), maximum daily tide height (a, blue dotted line) and their relationship (b). The heavy rainfall (a, gray columnar) events of DOY 215 occurred within one hour (between 04:00 pm and 05:00 pm). (Color figure online)



emissions were found. Missing hot moments in salt marshes could reduce estimates of daily emissions by up to 30%. However, there were very few studies using the EC technique to measure CH_4 emissions in tidal salt marshes (Holm et al. 2016). Thus, more measurements of CH_4 are required to quantify regional and global CH_4 budgets in the future.

Factors regulating F_{CH_4} at the tidal salt marsh

The control of tide on F_{CH_4}

Although tidal activities act as an important hydrological process in salt marshes, very few studies investigated the effect of tide on F_{CH_4} using the EC technique. Recently, one study reported 14 months of measurements from the Mississippi River Delta (Holm et al. 2016). However, they did not report the

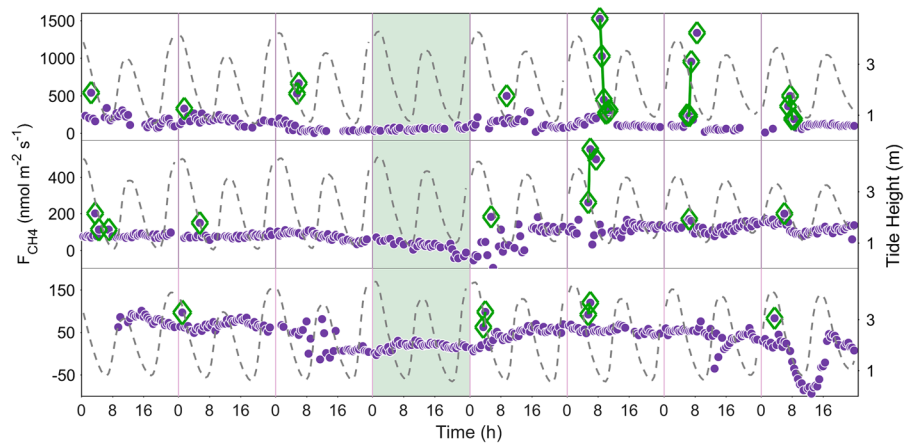


Fig. 9 The relationship of half-hourly (purple dot) methane flux (F_{CH_4}) without gap-filling and tide height (gray line) at diel scale in summer. The figures with light green background presented days of the spring tide (DOY186, 200, 213). Most of the hot moments (dark green diamond, greater than threefold

standard deviation + average of F_{CH_4} (hot-moment-points – average $> 3 \times \text{SD}$) within ± 6 h) occurred at 2–5 h after the nighttime high tide (convert to ebb tide) on 2–3 days before the spring tide and 1–4 days after the spring tide. (Color figure online)

relationship between F_{CH_4} and tide activities on semi-diurnal and semi-lunar scales.

Extreme high tide water levels reduced CH_4 emissions in the tidal salt marsh. A high water table usually enhances CH_4 production by providing anaerobic conditions and inhibiting root zone CH_4 aerobic oxidation. Indeed, there was some evidence showing that extended flooding could have minor or no significant effect on F_{CH_4} , as excess water can provide a direct barrier to the release of gases from the soil layer or the water column (Christensen et al. 2003; Heinsch et al. 2004; Long et al. 2010). In our case, we found that F_{CH_4} and tide height had a significant coherency at the half-to-one-month scale, with a negative correlation from June to September in 2011 (Fig. 4). The phase-locked domain indicated a cause-and-effect relationship. The tide height led F_{CH_4} by 0.7 days at the semi-lunar scale. In addition, the coherence at half-to-one-month scale was not confounded by weather variations in our case study (Fig S4). Moreover, the high-quality data of two full semi-lunar cycles of spring and neap tides clearly demonstrated that the effect of the tidal semi-lunar cycle on F_{CH_4} was significant (Fig. 8). This negative effect can be explained by several primary mechanisms. (1) When exposed soil layers were fully flooded, especially near the spring tide days, gas diffusion was hindered as the air space in the soil was replaced by water. (Tong et al. 2013; Yamamoto et al. 2009). (2)

Hydrostatic pressure decreased when water levels fell near the neap tide days, and the storage of CH_4 in the soil layers or water column could be released (Bubier and Moore 1994; Rosenqvist et al. 2002). Yet, further efforts to obtain more data of water table depth in the footprint areas are needed to better constrain the relationship of water table and methane emissions.

In addition, sulfate reduction may be another primary reason for the response of F_{CH_4} to the semi-lunar cycles of spring and neap tides. The variation of tide height was an indicator of tidal dynamics, which not only represented the variation of water level, but also indicated potential variations in the intertidal zone, such as sulfate content, soil temperature, and physical action of the tidal ebb and flow. The constant supply of SO_4^{2-} , which as a more favorable terminal electron acceptor by tidal exchange in tidal salt marshes, can suppress CH_4 production based on thermodynamics (Bartlett et al. 1987; Poffenbarger et al. 2011; Holm et al. 2016). The soil salinity and sulfate content increased from the neap tide to the spring tide at our study site (Bu 2013; Bu et al. 2015). Thus, the sulfate reduction can also explain why F_{CH_4} decreased from the neap tide to the spring tide (Fig. 8). One previous study conducted in the same area also concluded that the inhibition of methanogenesis by the increased soil salinity and sulfate was likely the primary reason of the decrease in soil CH_4 emissions during spring tide periods in the Dongtan wetland (Bu

et al. 2015). Furthermore, air temperature and GEP fluctuated in a narrow range during this period. We have also made a statistical tested and did not find any significant effect ($p > 0.05$) of any of the two variables on F_{CH_4} during this period, even after taking into account potential time lags.

Moreover, the ebbing of the tide led hot moments of CH_4 emissions on the days near the spring tide. We found a sharp increase in F_{CH_4} after the nighttime high tide on the days near the spring tide (Fig. 9). During the pulse day, the soil was almost saturated and thus favorable for CH_4 production. Considering that the transport by plants was weak at nighttime as there was no photosynthesis, diffusion and bubbling could be the primary transports of CH_4 at night in the marsh. However, excess water could constitute a direct barrier to gas diffusion and ebullition and then CH_4 would be stored in the water/soil layer near high tide on the days near the spring tide. The ebbing with a decrease of the water level can reduce the pressure on soil layer storing CH_4 and can help releasing the stored CH_4 from the water or soil in the marsh. Meanwhile, the pulse of CH_4 did not happen after the daytime high tide (Fig. 9). On the pulse days, the height of the daytime high tide was much lower than that of the nighttime high tide (Fig. S5). Thus, the difference between the nighttime and daytime emissions can be attributed to the difference (the daily inequality) in the height of the two high tides (Fig. S5). Additionally, the plant-mediated transport of CH_4 at daytime can play an important role in vascular plants, when soil layers were flooded with tide water near the high tide (Van Der Nat et al. 1998; Wang et al. 2009). Yet, it probably is not the dominant transport pathway when the soil is exposed as there was no consistent diel pattern of F_{CH_4} . Meanwhile, our multiple wavelet coherence analysis (Fig. 6) showed significant explanatory coherency at the diel scale when the tide height and PAR were combined. Thus, the plant-mediated transport of CH_4 at daytime which resulted in a small CH_4 storage in the water/soil layer would not lead to hot moments after the daytime high tide.

Influence of other factors on F_{CH_4}

Temperature, PAR, and GEP could be important factors regulating F_{CH_4} . Change in temperature is known to have a major effect on F_{CH_4} (Christensen et al. 2003; Rinne et al. 2007; Yvon-Durocher et al.

2014). The exponential dependence of F_{CH_4} on temperature (Fig. 7, $R^2 = 0.48, 0.56$ in 2011 and 2012, respectively) in the marsh was similar to that in many reported wetlands (Helbig et al. 2017; Homineltenberg et al. 2014; Rinne et al. 2007). In addition, significant relationships between F_{CH_4} and PAR, GEP have also been reported by a few studies (Chu et al. 2014; Hatala et al. 2012; Koebsch et al. 2015; Long et al. 2010). This could be attributed to the following processes: (1) the provision of photosynthates, which were subsequently used as substrates for methanogenic microbes (Chanton and Whiting 1996; Dorodnikov et al. 2011; Minoda and Kimura 1994); (2) plant-mediated transport, as increased radiation can increase stomatal conductance and promote the pressure-driven CH_4 transport via aerenchyma tissue of vascular plants (Brix et al. 1992). Hatala et al. (2012) found that GEP and F_{CH_4} show strong spectral coherency at the diurnal scale, which results in a diurnal pattern in methane emission from a Californian rice paddy. Koebsch et al. (2015) also found that PAR as a proxy for plant activity controls the variation of F_{CH_4} on a diel scale at the beginning of the growing season in a degraded fen. However, these pioneering multi-scale studies only covered one growing-season and were therefore not exploring the seasonal scale controls on F_{CH_4} .

Temperature, PAR, and GEP played different roles in regulating F_{CH_4} at each time scale in the tidal salt marsh. Although they were identified as F_{CH_4} controls in many studies, it is difficult to disentangle scale-specific confounding effects as they are characterized by similar cycles and patterns. In our study, the combination of WTC and PWC analyses has eliminated the confounding influences of T_a , PAR, and GEP on F_{CH_4} . The results show that air temperature was the most important control on F_{CH_4} compared to PAR, GEP, and tide height at the multi-day scale. In contrast, PAR and GEP rather than temperature were the dominating factors in regulating F_{CH_4} at the seasonal scale (Figs. 4 and 5). The variability of T_a was relatively strong (Fig. S3) in comparison to PAR and GEP, which can be a proxy for plant activity integrated over a few days. Meanwhile, the growth and phenology of *Phragmites australis* and *Spartina alterniflora* have clear seasonal variations. Therefore, carbon substrate supply was likely an important control on the magnitude of F_{CH_4} in the marsh. GEP was not significantly coherent to F_{CH_4} at the seasonal

scale in 2012, which may result from the large gaps and the uncertainty in the estimation of GEP. One study conducted in the same study area also reported that vegetation activity was one of the primary factors controlling F_{CH_4} during its growing stage (Wang et al. 2009). Yet, we cannot separate the contribution of PAR, which related to both transport and carbon supply of CH_4 . To better understand the mechanisms behind CH_4 processes, more experiments of gradient changes are required, e.g. tracing the source of CH_4 -C to separate the processes of transport and carbon supply of plants on CH_4 at the seasonal scale.

Limitations

Two limitations highlight ways in which the wavelet analyses could be improved. First, the time series length was not long enough to analysis the periodicity or coherence on the annual scale. However, many studies reported the annual exponential dependence of F_{CH_4} on temperature (Christensen et al. 2003; Long et al. 2010; Rinne et al. 2007). Therefore, in this study, we added the exponential regression analysis for temperature dependence on daily-averaged F_{CH_4} . Second, a large number of short gaps in F_{CH_4} may sometimes bias wavelet calculation at scales longer than the length of the gaps and therefore information at time scales shorter than the length of the gaps would be lost. However, gap-filling can bring artificial correlations that will contribute to wavelet common power or coherence. Thus, the F_{CH_4} we used for wavelet analysis was filled using the mean of the normalized data instead of using the ANN approach.

More auxiliary data can help understand the mechanisms of tidal effects. Water table and sulfate were both reported as important factors on seasonal methane fluxes in coastal wetlands. We did design a set of devices to measure water table depth and salinity around the EC tower. However, the sonde was often blocked by the sediment brought by the tide, and thus the sonde did not work continuously. Therefore, a new way or new instrument to measure water table is required.

Conclusions

For the first time, we combined the EC technique and wavelet analyses to investigate the dynamic of F_{CH_4}

and its multiple scale-specific temporal controls in a subtropical tidal salt marsh in China. The tidal salt marsh acted as a strong CH_4 source ($17.6 \pm 3.0 \text{ g C-CH}_4 \text{ m}^{-2} \text{ year}^{-1}$), which was larger than most reports from inland wetland sites. There was no consistent diurnal pattern of F_{CH_4} for the whole measurement period; thus, the periodicity at diel scale was relatively weak compared to that of F_{CO_2} . Interestingly, hot moments of CH_4 emissions were observed after the nighttime high tide (convert to ebb tide) on the days near spring tide in summer. In addition, periodic variations at the multi-day scale (e.g., 5.3 days), half-to-one-month scale (e.g., 10.7–21.3 days), and seasonal scales (between 42.7 and 170.7 days) were observed, which were significantly regulated by air temperature, tidal activities, and PAR (and GEP), respectively. Tide height had a negative effect on F_{CH_4} at the semilunar scale. Our findings indicated that CH_4 flux exhibited multiple periodicities and its controls varied with time scale; moreover, CH_4 flux was also strongly modified by the tide in this specific area. Our results call for incorporating tide in biogeochemical models to improve our ability to predict regional CH_4 budget.

Acknowledgements This research was financially supported by the National Natural Science Foundation of China (No. 31170450, 41571083), Shanghai Science and Technology Innovation Action Plan (No. 13JC1400400, 13231203503), Shanghai Committee of Science and Technology (14ZR1435100), and the research fund of the State Key Laboratory of Estuarine and Coastal Research (2015KYYW03). Thanks S.-Y. Li, Z.-F. Xu, Z.-M. Deng, Y. Min, B.-Q. Chen, J.-G. Gao, J. Ma, J. Xiong, Y. Hou for their helpful assistances and advices for the manuscript. Thanks J.-H. Li and L.-K. Xu (in LICOR) for technical support of flux calculations and co-spectral analysis by Eddypro. Thanks to J. H. Matthes for helpful suggestions on this manuscript. Thanks to M. Helbig for his professional revision of the English language. Thanks US-China Carbon Consortium (USCCC). H. Li thanks China Scholarship Council (CSC) for offering a scholarship at the University du Quebec at Montreal (UQAM). The authors would like to thank two anonymous reviewers for their constructive comments and suggestions.

References

- Baldocchi D (2014) Measuring fluxes of trace gases and energy between ecosystems and the atmosphere—the state and future of the eddy covariance method. *Glob Chang Biol* 20:3600–3609. <https://doi.org/10.1111/gcb.12649>
- Baldocchi D et al (2001) FLUXNET: a new tool to study the temporal and spatial variability of ecosystem-scale carbon

- dioxide, water vapor, and energy flux densities. *Bull Am Meteorol Soc* 82:2415–2434. [https://doi.org/10.1175/1520-0477\(2001\)082<2415:fantts>2.3.co;2](https://doi.org/10.1175/1520-0477(2001)082<2415:fantts>2.3.co;2)
- Bartlett KB, Bartlett DS, Harriss RC, Sebacher DI (1987) Methane emissions along a salt marsh salinity gradient. *Biogeochemistry* 4:183–202. <https://doi.org/10.1007/bf02187365>
- Bridgman SD, Cadillo-Quiroz H, Keller JK, Zhuang Q (2013) Methane emissions from wetlands: biogeochemical, microbial, and modeling perspectives from local to global scales. *Glob Chang Biol* 19:1325–1346. <https://doi.org/10.1111/gcb.12131>
- Brix H, Sorrel BK, Orr PT (1992) Internal pressurization and convective gas flow in some emergent. *Limnol Oceanogr* 37:1420–1433. <https://doi.org/10.4319/lo.1992.37.7.1420>
- Bu N-S (2013) Effects of semi-lunar tidal cycling on soil CO₂ and CH₄ emissions: a case study in the Yangtze River estuary. Fudan University, Shanghai
- Bu N-S et al (2015) Effects of semi-lunar tidal cycling on soil CO₂ and CH₄ emissions: a case study in the Yangtze River estuary, China. *Wetl Ecol Manag* 23(4):727–736. <https://doi.org/10.1007/s11273-015-9415-5>
- Bubier JL, Moore TR (1994) An ecological perspective on methane emissions from northern wetlands. *Trends Ecol Evol* 9:460–464. [https://doi.org/10.1016/0169-5347\(94\)90309-3](https://doi.org/10.1016/0169-5347(94)90309-3)
- Chanton JP, Whiting GJ (1996) Methane stable isotopic distributions as indicators of gas transport mechanisms in emergent aquatic plants. *Aquat Bot* 54:227–236. [https://doi.org/10.1016/0304-3770\(96\)01047-9](https://doi.org/10.1016/0304-3770(96)01047-9)
- Cheng X et al (2007) CH₄ and N₂O emissions from *Spartina alterniflora* and *Phragmites australis* in experimental mesocosms. *Chemosphere* 68:420–427. <https://doi.org/10.1016/j.chemosphere.2007.01.004>
- Cheng X, Luo Y, Xu Q, Lin G, Zhang Q, Chen J, Li B (2010) Seasonal variation in CH₄ emission and its ¹³C-isotopic signature from *Spartina alterniflora* and *Scirpus maritimus* soils in an estuarine wetland. *Plant Soil* 327:85–94. <https://doi.org/10.1007/s11104-009-0033-y>
- Chmura GL, Anisfeld SC, Cahoon DR, Lynch JC (2003) Global carbon sequestration in tidal, saline wetland soils. *Glob Biogeochem Cycles* 17(4):1111. <https://doi.org/10.1029/2002gb001917>
- Christensen TR et al (2003) Factors controlling large scale variations in methane emissions from wetlands. *Geophys Res Lett* 30(7):1414. <https://doi.org/10.1029/2002gl016848>
- Chu H, Chen J, Gottgens JF, Ouyang Z, John R, Czajkowski K, Becker R (2014) Net ecosystem methane and carbon dioxide exchanges in a Lake Erie coastal marsh and a nearby cropland. *J Geophys Res* 119:722–740. <https://doi.org/10.1002/2013jg002520>
- Dorodnikov M, Knorr KH, Kuzyakov Y, Wilmking M (2011) Plant-mediated CH₄ transport and contribution of photosynthates to methanogenesis at a boreal mire: a ¹⁴C pulse-labeling study. *Biogeosciences* 8:2365–2375. <https://doi.org/10.5194/bg-8-2365-2011>
- Foken T, Gockede M, Mauder M, Mahrt L, Amiro B, Munger W (2004) Post-field data quality control. In: Lee X, Massman W, Law B (eds) *Handbook of micrometeorology: a guide for surface flux measurement and analysis*, vol 29. Kluwer Academic Publishers, Dordrecht, pp 181–208
- Granberg G, Mikkela C, Sundh I, Svensson BH, Nilsson M (1997) Sources of spatial variation in methane emission from mires in northern Sweden: a mechanistic approach in statistical modeling. *Glob Biogeochem Cycles* 11:135–150. <https://doi.org/10.1029/96gb03352>
- Grinsted A, Moore JC, Jevrejeva S (2004) Application of the cross wavelet transform and wavelet coherence to geophysical time series. *Nonlinear Process Geophys* 11:561–566. <https://doi.org/10.5194/npg-11-561-2004>
- Hatala JA, Detto M, Baldocchi DD (2012) Gross ecosystem photosynthesis causes a diurnal pattern in methane emission from rice. *Geophys Res Lett* 39(6):L06409. <https://doi.org/10.1029/2012gl051303>
- Heinsch F, Heilman J, McInnes K, Cobos D, Zuberer D, Roelke D (2004) Carbon dioxide exchange in a high marsh on the Texas Gulf Coast: effects of freshwater availability. *Agric For Meteorol* 125:159–172. <https://doi.org/10.1016/j.agrformet.2004.02.007>
- Helbig M, Chasmer LE, Kljun N, Quinton WL, Treat CC, Sonntag O (2017) The positive net radiative greenhouse gas forcing of increasing methane emissions from a thawing boreal forest-wetland landscape. *Glob Chang Biol* 23:2413–2427. <https://doi.org/10.1111/gcb.13520>
- Holm GO, Perez BC, McWhorter DE, Krauss KW, Johnson DJ, Raynie RC, Killebrew CJ (2016) Ecosystem level methane fluxes from tidal freshwater and brackish marshes of the Mississippi River Delta: implications for coastal wetland carbon projects. *Wetlands* 36:401–413. <https://doi.org/10.1007/s13157-016-0746-7>
- Homineltenberg J, Mauder M, Drosler M, Heidebach K, Werle P, Schmid HP (2014) Ecosystem scale methane fluxes in a natural temperate bog-pine forest in southern Germany. *Agric For Meteorol* 198:273–284. <https://doi.org/10.1016/j.agrformet.2014.08.017>
- IPCC (2013) IPCC, 2013: climate change 2013: the physical science basis. Contribution of working group I to the fifth assessment report of the intergovernmental panel on climate change. Cambridge University Press,
- Järvi L, Nordbo A, Junninen H, Riikonen A, Moilanen J, Nikinmaa E, Vesala T (2012) Seasonal and annual variation of carbon dioxide surface fluxes in Helsinki, Finland, in 2006–2010. *Atmos Chem Phys* 12:8475–8489. <https://doi.org/10.5194/acp-12-8475-2012>
- Kirschke S et al (2013) Three decades of global methane sources and sinks. *Nat Geosci* 6:813–823. <https://doi.org/10.1038/ngeo1955>
- Koebisch F, Jurasinski G, Koch M, Hofmann J, Glatzel S (2015) Controls for multi-scale temporal variation in ecosystem methane exchange during the growing season of a permanently inundated fen. *Agric For Meteorol* 204:94–105. <https://doi.org/10.1016/j.agrformet.2015.02.002>
- Long KD, Flanagan LB, Cai T (2010) Diurnal and seasonal variation in methane emissions in a northern Canadian peatland measured by eddy covariance. *Glob Chang Biol* 16:2420–2435. <https://doi.org/10.1111/j.1365-2486.2009.02083.x>
- Mihanović H, Orlić M, Pasarić Z (2009) Diurnal thermocline oscillations driven by tidal flow around an island in the

- Middle Adriatic. *J Mar Syst* 78:S157–S168. <https://doi.org/10.1016/j.jmarsys.2009.01.021>
- Minoda T, Kimura M (1994) Contribution of photosynthesized carbon to the methane emitted from paddy fields. *Geophys Res Lett* 21:2007–2010. <https://doi.org/10.1029/94gl01595>
- Neubauer SC, Franklin RB, Berrier DJ (2013) Saltwater intrusion into tidal freshwater marshes alters the biogeochemical processing of organic carbon. *Biogeosciences* 10:8171–8183. <https://doi.org/10.5194/bg-10-8171-2013>
- Ng EK, Chan JC (2012) Geophysical applications of partial wavelet coherence and multiple wavelet coherence. *J Atmos Ocean Technol* 29:1845–1853. <https://doi.org/10.1175/jtech-d-12-00056.1>
- Nicolini G, Castaldi S, Fratini G, Valentini R (2013) A literature overview of micrometeorological CH₄ and N₂O flux measurements in terrestrial ecosystems. *Atmos Environ* 81:311–319. <https://doi.org/10.1016/j.atmosenv.2013.09.030>
- Ouyang Z, Chen J, Becker R, Chu H, Xie J, Shao C, John R (2014) Disentangling the confounding effects of PAR and air temperature on net ecosystem exchange at multiple time scales. *Ecol Complex* 19:46–58. <https://doi.org/10.1016/j.ecocom.2014.04.005>
- Papale D, Valentini R (2003) A new assessment of European forests carbon exchanges by eddy fluxes and artificial neural network spatialization. *Glob Chang Biol* 9:525–535. <https://doi.org/10.1046/j.1365-2486.2003.00609.x>
- Poffenbarger HJ, Needelman BA, Megonigal JP (2011) Salinity influence on methane emissions from tidal marshes. *Wetlands* 31:831–842. <https://doi.org/10.1007/s13157-011-0197-0>
- Reichstein M et al (2005) On the separation of net ecosystem exchange into assimilation and ecosystem respiration: review and improved algorithm. *Glob Chang Biol* 11(9): 1424–1439. <https://doi.org/10.1111/j.1365-2486.2005.001002.x>
- Rinne J et al (2007) Annual cycle of methane emission from a boreal fen measured by the eddy covariance technique. *Tellus B* 59:449–457. <https://doi.org/10.1111/j.1600-0889.2007.00261.x>
- Rosenqvist Å, Forsberg B, Pimentel T, Rauste Y, Richey J (2002) The use of spaceborne radar data to model inundation patterns and trace gas emissions in the central Amazon floodplain. *Int J Remote Sens* 23:1303–1328. <https://doi.org/10.1080/01430060110092911>
- Stoy PC et al (2005) Variability in net ecosystem exchange from hourly to inter-annual time scales at adjacent pine and hardwood forests: a wavelet analysis. *Tree Physiol* 25:887–902. <https://doi.org/10.1093/treephys/25.7.887>
- Sturtevant C, Ruddell BL, Knox SH, Verfaillie J, Matthes JH, Oikawa PY, Baldocchi D (2015) Identifying scale-emergent, nonlinear, asynchronous processes of wetland methane exchange. *J Geophys Res* 121(1):188–204. <https://doi.org/10.1002/2015jg003054>
- Sun Z, Jiang H, Wang L, Mou X, Sun W (2013a) Seasonal and spatial variations of methane emissions from coastal marshes in the northern Yellow River estuary, China. *Plant Soil* 369:317–333. <https://doi.org/10.1007/s11104-012-1564-1>
- Sun Z, Wang L, Tian H, Jiang H, Mou X, Sun W (2013b) Fluxes of nitrous oxide and methane in different coastal Sueda salsa marshes of the Yellow River estuary, China. *Chemosphere* 90:856–865. <https://doi.org/10.1016/j.chemosphere.2012.10.004>
- Tong C, Wang W-Q, Zeng C-S, Marrs R (2010) Methane (CH₄) emission from a tidal marsh in the Min River estuary, southeast China. *J Environ Sci Health Part A* 45:506–516. <https://doi.org/10.1080/10934520903542261>
- Tong C, Huang JF, Hu ZQ, Jin YF (2013) Diurnal variations of carbon dioxide, methane, and nitrous oxide vertical fluxes in a subtropical estuarine marsh on neap and spring tide days. *Estuaries Coasts* 36:633–642. <https://doi.org/10.1007/s12237-013-9596-1>
- Van Der Nat F-FW, Middelburg JJ, Van Meteren D, Wielemakers A (1998) Diel methane emission patterns from *Scirpus lacustris* and *Phragmites australis*. *Biogeochemistry* 41(1):1–22. <https://doi.org/10.1023/a:1005933100905>
- Vargas R, Detto M, Baldocchi DD, Allen MF (2010) Multiscale analysis of temporal variability of soil CO₂ production as influenced by weather and vegetation. *Glob Chang Biol* 16:1589–1605. <https://doi.org/10.1111/j.1365-2486.2009.02111.x>
- Wang D, Chen Z, Xu S (2009) Methane emission from Yangtze estuarine wetland, China. *J Geophys Res* 114(G2):1588–1593
- Weston NB, Neubauer SC, Velinsky DJ, Vile MA (2014) Net ecosystem carbon exchange and the greenhouse gas balance of tidal marshes along an estuarine salinity gradient. *Biogeochemistry* 120:163–189. <https://doi.org/10.1007/s10533-014-9989-7>
- Windsor J, Moore T, Roulet N (1992) Episodic fluxes of methane from subarctic fens. *Can J Soil Sci* 72:441–452. <https://doi.org/10.4141/cjss92-037>
- Xie X, Zhu WB, Guo HQ, Zhao B (2013) Tides and rainfall affected water table depth of coastal wetland. *J Fudan Univ (Nat Sci)* 52(6):801–806
- Xu L, Lin X, Amen J, Welding K, McDermitt D (2014) Impact of changes in barometric pressure on landfill methane emission. *Glob Biogeochem Cycles* 28:679–695. <https://doi.org/10.1002/2013gb004571>
- Yamamoto A, Hirota M, Suzuki S, Oe Y, Zhang P, Mariko S (2009) Effects of tidal fluctuations on CO₂ and CH₄ fluxes in the littoral zone of a brackish-water lake. *Limnology* 10:229–237. <https://doi.org/10.1007/s10201-009-0284-6>
- Yang S-L, Ding P-X, Chen S-L (2001) Changes in progradation rate of the tidal flats at the mouth of the Changjiang (Yangtze) River, China. *Geomorphology* 38:167–180. [https://doi.org/10.1016/s0169-555x\(00\)00079-9](https://doi.org/10.1016/s0169-555x(00)00079-9)
- Yvon-Durocher G et al (2014) Methane fluxes show consistent temperature dependence across microbial to ecosystem scales. *Nature* 507:488–491. <https://doi.org/10.1038/nature13164>
- Zhao B, Guo HQ, Yan Y, Wang Q, Li B (2008) A simple waterline approach for tidelands using multi-temporal satellite images: a case study in the Yangtze Delta Estuarine. *Coast Shelf Sci* 77:134–142. <https://doi.org/10.1016/j.cess.2007.09.022>